Chemical Research in Toxicology

Article

pubs.acs.org/crt

Glycophthalocyanines as Photosensitizers for Triggering Mitotic Catastrophe and Apoptosis in Cancer Cells

Ana R. M. Soares,[†,‡] Maria G. P. M. S. Neves,[†] Augusto C. Tomé,[†] M. Carmen Iglesias-de la Cruz,[§] Alicia Zamarrón,[§] Elisa Carrasco,[§] Salvador González,[∥] José A. S. Cavaleiro,[†] Tomás Torres,[‡] Dirk M. Guldi,[⊥] and Angeles Juarranz*[,§]

[†]Universidade de Aveiro, Departamento de Química, QOPNA, 3810-193 Aveiro, Portugal

[‡]Departamento de Química Orgánica, Facultad de Ciencias, Universidad Autónoma de Madrid, IMDEA Nanociencia, Cantoblanco 28049 Madrid, Spain

[§]Departamento de Biología, Facultad de Ciencias, Universidad Autónoma de Madrid, Cantoblanco 28049, Madrid, Spain

[∥]Dermatology Service, Memorial Sloan-Kettering Cancer Center, New York, United States

[⊥]Friedrich-Alexander-Universität Erlangen-Nürnberg, Department of Chemistry and Pharmacy & Interdisciplinary Center for Molecular Materials (ICMM), 91058, Erlangen, Germany

S *Supporting Information*

ABSTRACT: Photodynamic therapy (PDT) is a treatment modality for different forms of cancer based on the combination of light, molecular oxygen, and a photosensitizer (PS) compound. When activated by light, the PS generates reactive oxygen species leading to tumor destruction. Phthalocyanines are compounds that have already shown to be efficient PSs for PDT. Several examples of carbohydrate substituted phthalocyanines have been reported, assuming that the presence of carbohydrate moieties could improve their tumor selectivity. This work describes the photoeffects of symmetric and asymmetric phthalocyanines with D-galactose (so-called GPh1, GPh2, and GPh3) on HeLa carcinoma cells and their involvement in cell death. Photophysical properties and *in vitro* photodynamic activities for the compounds considered revealed that the asymmetric glycophthalocyanine GPh3 is very efficient and selective, producing higher photocytotoxicity on cancer cells than in nonmalignat HaCaT. The cell toxiticy after PDT treatment was dependent upon light exposure level and GPh3 concentration. GPh3 causes cell cycle arrest at the metaphase stage leading to multiple spindle poles, mitotic catastrophe, followed by apoptosis in cancer cells. These effects were partially negated by the pancaspase inhibitor Z-VAD-FMK. Together, these results indicate that GPh3 is an excellent candidate drug for PDT, able to induce selective tumor cell death.

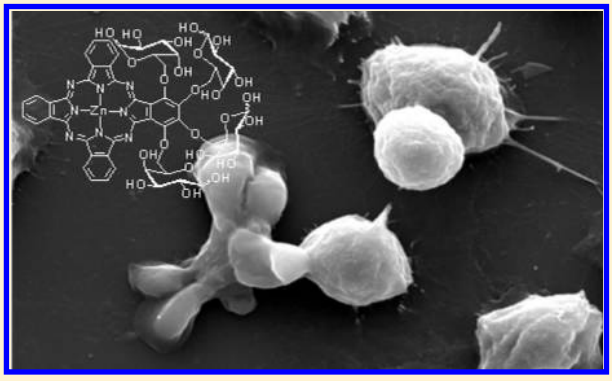

1. INTRODUCTION

Photodynamic therapy (PDT) is a treatment modality for several types of cancer,[1−3] and it involves the combination of three key components: light, molecular oxygen, and a photosensitizer (PS), each component being harmless by itself. The treatment begins with the administration to the patient of a PS, which selectively accumulates in the tumor tissue. The PS is then illuminated with visible light of a specific wavelength, typically in the red region of the spectrum (620−690 nm), as the red light penetrates deeper into tissues. Usually, the PS is excited from a ground singlet state to an excited singlet state and later on to a longer-lived excited triplet state. When the PS and an oxygen molecule are in proximity, energy transfer takes place between them, so the PS relaxes to its ground singlet state, and different reactive oxygen species (ROS), mainly singlet oxygen ($^1O_2$), are generated. Singlet oxygen is a highly toxic molecule, which reacts rapidly with several biologically important substrates leading to significant oxidative damage and to the destruction of tumors. Tumor destruction by PDT is achieved directly by causing cellular damage or indirectly through injuring tumor vasculature. Moreover, PDT can also activate the immune response against tumor cells.[1−3] Cell components that can be targets for PDT include plasma membrane, lysosomes, mitochondria, Golgi apparatus, endoplasmic reticulum, nuclei, and also cytoskeleton and cell adhesion components.[3] Targeting the cytoskeleton is an important goal for anticancer therapies, including PDT, since the cytoskeleton plays significant roles in processes related with tumor progression such as cell motility, division, and vesicular transport. Indeed, microtubules (MTs) and microfilaments (MFs) are essential targets in chemotherapy with anticancer compounds such as Vinca and Colchicum alkaloids, criptophycins, nocodazole, epothilones, and taxoids.[4] MTs have been

Received: January 26, 2012
Published: March 6, 2012

   dx.doi.org/10.1021/tx300035a | *Chem. Res. Toxicol.* 2012, 25, 940−951

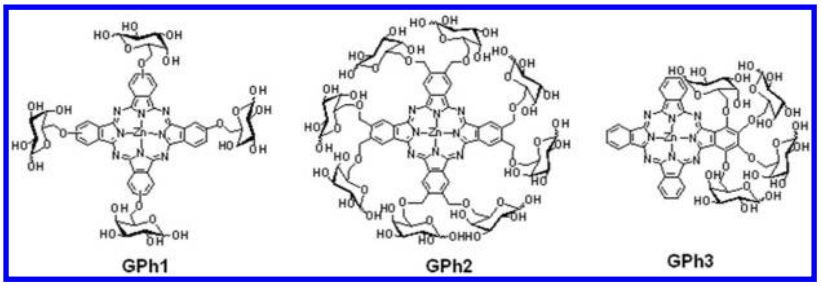

Figure 1. Chemical structures of the glycophthalocyanines. The PS compounds were abbreviated as GPh1, GPh2, and GPh3.

described to be altered after PDTs using different porphyrins, phthalocyanines, and porphycenes as PSs.[5−9] In addition, such treatments were able to induce cell cycle blockage at the metaphase−anaphase transition, which led to mitotic catastrophe followed by apoptosis.[10,11]

Different studies have been focused on the development and efficacy of new PSs, with improved photophysical and photobiological properties, and a large number of PSs based on porphyrin- and phthalocyanine-derivatives have been developed.[12−15] Phthalocyanine derivatives exhibit several optimal characteristics for being good PSs: (i) a high molar absorption coefficient ($\varepsilon > 10^5$ $M^{-1}cm^{-1}$) in the visible region of the spectrum; (ii) a long lifetime of the triplet excited state; and (iii) an increased oxidative stability that allows their use as stable aqueous solutions. We and others have demonstrated the photosensitizing effects of zinc(II) phthalocyanines (ZnPc) both *in vivo*, for treatment of mice tumors,[16] and *in vitro*, for induction of cytotoxic effect on several cell lines.[6,7,17] Moreover, liposomal ZnPc has been applied in phase I/II clinical trials for the treatment of skin, oropharingeal, lung, larynx, and gastrointestinal neoplasias, as well as psoriasis.[13,18] It is then noticeable that great scientific attention has been focused on the study of new ZnPc derivatives in the past years.[19−21]

Nevertheless, one important problem of phthalocyanine compounds is the insolubility of their hydrophobic skeleton in physiological fluids. In order to provide water solubility, neutral and ionic phthalocyanine derivatives bearing diverse polar hydrophilic substituents at the periphery of the molecule have been reported.[22−25] A suitable combination of hydrophilic and hydrophobic substituents or structural elements is required in order to fine-tune the amphiphilicity of the resulting conjugates and then improve the tumor uptake.[14,19,26] Amphiphilic PSs have proved to be more photodynamically active since they can localize at the hydrophobic−hydrophilic interfaces of membranes, interacting with the surface of proteins. Amphiphilic compounds are useful for Photochemical Internalization (PCI), a quite new technology for drug delivery, which is based on the activation of an amphiphilic PS by light to release chemotherapeutic compounds inside the cell.[27,28] Additionally, amphiphilicity can also affect the degree to which a compound aggregates, therefore affecting the photophysical properties of the PS, as aggregation shortens the triplet-state lifetime and decreases the singlet oxygen quantum yield by dissipating the energy through internal conversion.[13,19,29]

A great deal of scientific attention has been focused on the development of novel PS with good biodistribution and localization properties toward a more effective photodynamic activity.[12,29,30] It is known that cancer cells have increased levels of glucose uptake and glycolysis in order to provide sufficient metabolic energy to sustain their proliferation. By taking advantage of this fact, the combination of carbohydrate moieties with macrocycles has attracted considerable interest, with the aim of enhancing their cellular uptake and eventually the PDT efficacy.[24,26,31] Recently, glycosylated silicon(IV) and zinc(II) phthalocyanines present photodynamic activities, and promising results *in vitro* have been observed for the asymmetrically conjugated analogues.[24,32,33] In addition, there are several works indicating that many cancer cells express high sugar receptors such as galectin with preferential affinity for galactose residues.[33,34]

Herein we describe the photodynamic effects of symmetric and asymmetric phthalocyanines bearing D-galactose units (Figure 1) on HeLa carcinoma cells and their involvement in cell death. The photophysical properties of the glycophthalocyanines (GPh) are also reported.

2. MATERIALS AND METHODS

2.1. Synthesis and Photophysical Properties of Glycophthalocyanines. The three glycophthalocyanines (GPhs) were synthesized as previously reported by Soares et al.[25] and Ribeiro et al.[23] The fluorescence quantum yields (Φ_F) in toluene and dimethyl sulfoxide (DMSO) were calculated by the comparative method of Williams et al.,[35] using ZnPc as the standard (Φ_F = 0.30). The singlet oxygen quantum yields (Φ_Δ) of the three glycophthalocyanines were determined by fluorescence spectroscopy using a Horiba Jobin Yvon Fluorolog-3 spectrophotometer TCSPC (Time-Correlated Single-Photon Counting), equipped with a 450 W xenon lamp, TRIAX 320 iHR emission spectrograph, and near-IR accessories (SIGA-Symphony InGaAs array detectors 800−1700 nm and emission grating at 100 × 780 nm). This system easily detects the near-IR emission of singlet oxygen signal (around 1280 nm). Quantum yields of singlet oxygen were determined in air-saturated DMSO solutions.[35]

2.2. Cell Culture. For the *in vitro* studies, we used cultured HeLa cells, a p53-deficient human epithelial carcinoma cell line. For the toxicity experiments, we also used HaCaT cells, a spontaneously transformed but nontumorogenic human keratinocytes cell line. Both cell types were routinely grown as a monolayer in F25 flasks (Costar, Corning, NY, USA) on culture dishes with or without glass coverslips placed inside the dishes, using Dulbecco's modified Eagle's medium (DMEM) supplemented with 10% (v/v) fetal bovine serum (FBS), 50 units/mL penicillin, 50 μg/mL streptomycin, and 1% (v/v) 0.2 M L-glutamine (all from Gibco, Paisley, Scotland, UK) (complete medium). Cell cultures were performed in an incubator with 5% of CO_2 at 37 °C. In all cases, subconfluent cell cultures (70−80%) were used.

2.3. Preparation of GPhs and Incubation of Cells. Stock solutions of GPhs (8×10^{-4} M) were prepared in DMSO (Panreac, Barcelona, Spain). Work solutions for cell incubations were prepared from the stock solutions using DMEM with 10% FBS. The final concentration of DMSO was always lower than 0.5% (v/v), and the lack of toxicity of this DMSO concentration for HeLa and HaCaT cells was tested and confirmed.

2.4. Subcellular Localization of GPhs. In order to analyze the localization of the GPhs inside the cells, HeLa cells were grown on coverslips. When cells reached around 70% of confluence, they were

dx.doi.org/10.1021/tx300035a | *Chem. Res. Toxicol.* 2012, 25, 940−951

incubated with GPh1, GPh2, or GPh3 either for 4 or 18 h at 37 °C. Then, cells were washed with PBS, mounted on slides, and observed *in situ* with a fluorescence microscope using an excitation light between 460 and 490 nm. The subcellular localization was analyzed comparing the fluorescent signal pattern emitted by the compounds with that obtained by fluorescent markers of selective subcellular accumulation: MitoTracker Green (MTG) for mitochondria, Lysotracker Green (LTG) for lysosomes, and NBD C6-ceramide or CellLight Golgi-GFP for Golgi apparatus (all of them from Invitrogen, California, USA) following the instructions of the commercial procedures. We also analyzed the colocalization of GPh3 (λ_{ex} = 460−90 nm) with the markers (λ_{ex} = 545−80 nm). For that, cells were incubated with GPh3 5×10^{-7} M for 4 or 18 h, the medium containing GPh3 was discarded, and the cells were further incubated for 5 min with medium containing Mitotracker or Lisotracker Green. For Golgi apparatus colocalization studies, cells were coincubated with GPh3 and CellLight Golgi-GFP for 18 h. The colocalization assays were performed twice and evaluated using the Olympus fluorescence microscope and the appropriate filter sets described in section 2.10.

2.5. Photodynamic Treatments. The protocols followed for these experiments are published elsewhere.[6,11,36] Briefly, HeLa or HaCaT cells were incubated with variable concentrations of PSs, ranging from 1×10^{-8} M to 1×10^{-6} M, for 4 h. After incubation, cells were washed with PBS and then irradiated in complete media at 6.2 mW/cm^2 for variable times (5 to 30 min corresponding to light doses from 1.86 to 11.16 J/cm^2) with a red light emitting diode source (LED, WP7143 SURC/E) with an emission peak at $\lambda = 634 \pm 20$ nm, as measured with a spectrophotometer. In some experiments, HeLa cells were also incubated with 30 μM (final concentration) of the broad-spectrum caspase inhibitor benzylocarbonyl-Val-Ala-Asp-fluoromethyl ketone (Z-VAD-fmk) (BD Pharmigen) for 4 h in the presence of the PS (GPh3) before light irradiation. The cells, after irradiation were incubated in DMEM complete media for selected time points in the incubator at 37 °C.

2.6. Cellular Toxicity. Toxicity of the different concentrations of GPh compounds on HeLa and HaCaT cells was evaluated 48 h after photodynamic treatment by the MTT (3-(4,5-dimethylthiazol-2-yl)-2,5-diphenyltetrazolium bromide, Sigma, St Louis, MI, USA) assay. This method is widely accepted as a quantitative colorimetric assay for mammalian cell toxicity[37] based on active cell metabolism. A stock MTT solution (1 mg/mL) in PBS (Dulbecco's Phosphate-Buffered Saline, Gibco) was prepared immediately prior to use. Then, a solution of MTT with DMEM (10% FBS) was prepared (1 mL MTT-PBS/10 mL DMEM), and 500 μL of this solution was added to the culture dishes. After incubation at 37 °C for 3 h, the culture medium was removed, and the precipitated formazan was dissolved in 500 μL of DMSO per well. The absorption was measured at 542 nm in a spectrophotometer (Espectra Fluor 4, Tecan). Cellular toxicity was expressed as a percentage of formazan absorption from PS-treated cells compared to control cells (which received neither PS nor PDT). To test the effect of light only on cell toxicity, we performed control experiments using only the red light irradiation on cells (636 nm) for 30 min, the most prolonged irradiation time used in this work. The results obtained are mean values and standard deviations from three independent experiments.

2.7. Morphological Studies. HeLa cells were grown in coverslips until 70−80% confluence. Changes in cell morphology 3, 24, and 48 h after photodynamic treatment (5×10^{-7} M of GPh3 for 4 h and a light dose of 5.58 J/cm^2) were analyzed using bright field illumination, fluorescence microscopy under UV excitation, or scanning electron microscopy. For general morphology, cells were fixed in cold methanol (−20 °C) for 7 min, air-dried, and stained with 1 μg/mL Hoescht-33258 dye (H-33258) (Sigma) for 5 min for fluorescence observations. After washing with distilled water and air drying, preparations were mounted with DePeX (Serva, Heidelberg, Germany). For scanning electron microscopy (SEM), cells were fixed in 3% glutaraldehyde (Taab Laboratories, Berkshire, UK) for 1 h at room temperature and postfixed in 1% osmium tetroxide (Taab Laboratories) for 1 h at room temperature. After fixation, cells were taken through a graded alcohol dehydration series, placed in a critical point dryer, and viewed on the SEM.

2.8. Immunostaining. HeLa cells were grown in coverslips until 70−80% confluence. For the MTs study, 3, 24, and 48 h after photodynamic treatment (5×10^{-7} M of GPh3 for 4 h and a light dose of 5.58 J/cm^2), cells were fixed in cold methanol and incubated with primary mouse monoclonal antibody anti-α-tubulin (Sigma) at 1:50 dilution in PBS/Bovine Serum Albumin (BSA) for 1 h at 37 °C, inside a humid chamber. After washing with PBS, cells were incubated with 50 μL of the secondary antibody, fluorescein isothiocyanate (FITC)-labeled goat antimouse IgG (Interchim, Montluçon, Fance) at 1:250 dilution in PBS/BSA for 1 h at 37 °C, inside a humid chamber. Mitotic index (MI) was determined using the coverslips processed for immunodetection of MTs and counting cells in division (prophase, metaphase and anaphase-telophase). At least 1000 cells were counted for MI. Metaphases were divided in normal or abnormal configuration, depending on whether the spindle apparatus was clearly altered. The total number of counted cells in metaphase was ≥100 for each point.

For MFs detection, cells grown on coverslips were fixed in 3.7% paraformaldehyde for 30 min at 4 °C, and permeabilized with 0.1% Triton X-100 in PBS (v/v) for 30 min at room temperature. Afterward, cells were incubated with 50 μL of Phalloidin (Sigma, 0.5% Phalloidin diluted 1:90 in PBS/BSA) for 30 min at room temperature. Finally, nuclei were stained with H-33258 for 5 min and mounted with Vectashield (Vector Laboratories, California, USA).

2.9. TUNEL Assay. The TUNEL assay was used to detect DNA strand nicking on cells. Cells grown on coverslips were subjected to PDT and at determined times after treatment, and attached cells were directly fixed in 3.7% formaldehyde for 30 min at room temperature and permeabilized with 0.1% Triton X-100 in PBS (v/v) for 2 min. Cells were subjected to the TUNEL reaction: 50 μL of TUNEL label/TUNEL enzyme (Roche,1:10) for 1 h at 37 °C, using a humid chamber. Afterward, nuclei were stained with H-33258 for 5 min and mounted with Vectashield (Vector Laboratories). Detached cells were directly gathered from the culture supernatants, centrifuged (1,200 rpm, 5 min), resuspended in 3.7% formaldehyde, and processed for the TUNEL reaction.

2.10. Optical and Electron Microscopy. Microscopic observations were carried out using an Olympus BX61 epifluorescence microscope equipped with filter sets for fluorescence microscopy: ultraviolet (UV, 365 nm, exciting filter UG-1), blue (450−490 nm, exciting filter BP 490), and green (545 nm, exciting filter BP 545). Photographs were obtained with the digital camera Olympus DP50 and processed using the Adobe PhotoShop 7.0 software (Adobe Systems). Scanning electron microscopy was carried out using a Hitachi S-3000N, with an attached energy-dispersive X-ray (EDX) analyzer Oxford Instruments, model INCAx-sight.

2.11. Flow Cytometry. Culture flasks with near confluent cells after phototreatment (5×10^{-7} M of GPh3 for 4 h and a light dose of 5.58 J/cm^2) were trypsinized and, together with the supernatant to collect dead cells, centrifuged at 1800 rpm for 10 min and fixed with cold 70% (v/v) ethanol (−20 °C). Immediately prior to measurement, cells were concentrated by centrifugation for 10 min (2500 rpm) and resuspended with RNase solution (Sigma), and DNA was stained with propidium iodide (Sigma). Measurements were taken on a Beckman Coulter EPICS XL-MCL flow cytometer with an argon laser line at 488 nm complemented with appropriate filters.

2.12. Western Blot. Semiconfluent monolayers of cells after phototreatment (5×10^{-7} M of GPh3 for 4 h and a light dose of 5.58 J/cm^2) were washed and then lysed with RIPA buffer (150 mM NaCl, 1% Triton X-100, 0.05% deoxycholate, 0.1% SDS, 1% Nonidet-40, and 50 mM Tris, pH 8) containing Phosphatase cocktail 2 and Protease inhibitor cocktail (Sigma, St Louis, MI, USA). The samples were adjusted to the same protein concentration (Bichinconinic Acid Protein Assay Kit, Pierce, Rockford, IL, USA) and denatured by boiling in Laemmli sample buffer with 5% β-mercaptoethanol. Approximately 30 μg of each sample was subjected to electrophoresis separation in SDS−PAGE. Gels were then transferred to a PDVF Immobilon-P membrane (Millipore, Bedford, MA, USA) for 2 h and blocked with 2% nonfat milk in Tris-buffered saline (10 mM Tris−

Table 1. Basic Photophysical Properties of the Synthesized Glycophthalocyanines Measured in DMSO and Relative to ZnPc[a]

GPh	λ_{max} (nm (log ε))	λ_{em} (nm)[b]	λ_{ex} (nm)[c]	τ_F (±SD)	Φ_F[d] (±SD)	Φ_Δ[e] (±SD)
1	359 (4.91), 616 (4.55), 682 (5.20)	692	678	2.81 (±2.0 × 10^{-3})	0.23 (±0.01)	0.82 (±0.07)
2	357 (4.85), 618 (4.56), 682 (5.22)	690	679	2.87 (±2.0 × 10^{-3})	0.20 (±0.03)	0.76 (±0.06)
3	343 (4.54), 622 (4.44), 689 (5.23)	695	686	2.41 (±1.9 × 10^{-3})	0.21 (±0.03)	0.69 (±0.03)

[a]The fluorescence quantum yields (Φ_F) of the three PSs were quite similar (Φ_F around 0.2). All of these phthalocyanines are efficient singlet oxygen generators, particularly GPh1 and GPh2 with high values of quantum yields of singlet oxygen (Φ_Δ). [b]Excitation wavelength at 610 nm. [c]Emission wavelength at 710 nm. [d]Relative to ZnPc in toluene (Φ_F = 0.30 ± 0.06). [e]Relative to ZnPc in DMSO (Φ_Δ = 0.67 ± 0.04).

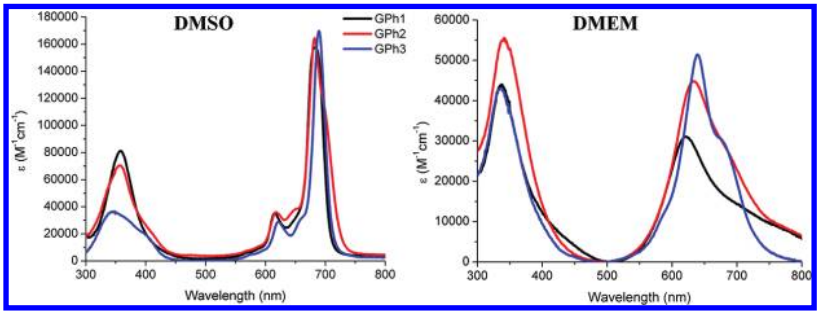

Figure 2. Electronic absorption spectra of the glycophthalocyanines. In DMSO, all of these compounds gave the typical UV−vis spectra for nonaggregated phthalocyanines with an intense and sharp Q-band in the red visible region and a Soret band at about 350 nm (left panel). The aggregation behavior of these compounds in the culture media (DMEM with 10% of FBS) is also shown (right panel); the Q-band of all compounds are much broadened and shifted to the blue, indicating that these compounds are to some extent aggregated in the medium.

HCl at pH 7.6, 0.9% NaCl, and 0.05% Tween 20). After blocking, membranes were incubated for 2 h at room temperature with specific primary mouse monoclonal antibodies against poly ADP-ribose polymerase (PARP), caspase-3, G-actin (Transduction Laboratories, Franklin Lakes, NJ, USA), cyclin B1 (Biosource International, Camarillo, CA, USA), or cyclin D1 (Novocastra, NEW Castle, UK). Membranes were finally washed with fresh PBS (3 times, 5 min each), incubated with the peroxidase-conjugated secondary sheep antimouse IgG (Amersham Pharmacia Biotech, Piscataway, NJ), and developed by chemiluminescence (ECL, Amersham). All antibodies were used at the concentrations recommended by the manufacturers. Bands corresponding to different proteins were quantified by scanning of photographs and then digitalized and analyzed with Adobe Photoshop CS by densitometry.

2.13. Statistical Analysis. Data are expressed as the mean value ± standard deviations (SD). The statistical significance was determined using t test and analysis of variance (ANOVA), and $p < 0.01$ was considered statistically significant.

3. RESULTS

3.1. Photophysical Properties and Electronic Absorption of the Synthesized Glycophthalocyanines. The basic photophysical data of the glycophthalocyanines (Figure 1), measured in DMSO, as well as their electronic absorption spectra in DMSO and DMEM are shown in Table 1 and Figure 2. Fluorescence quantum yields (Φ_F) were calculated by the comparative method of Williams et al.,[35] using ZnPc as the standard (Φ_F = 0.30 ± 0.06). The fluorescence quantum yields of the three PSs were quite similar (Φ_F around 0.2). In time-resolved fluorescence measurements, the lifetime (τ_F) emerged for ZnPc at 647 nm was 2.8 ns, and similar values were obtained for the fluorescence τ_F of the PSs studied. These data are compiled and shown in Table 1. It can be seen that in DMSO all of these phthalocyanines are efficient singlet oxygen generators, particularly GPh1 and GPh2, for which the values of singlet oxygen quantum yields, Φ_Δ (0.82 ± 0.07 and 0.76 ± 0.06, respectively), are higher than that of ZnPc (Φ_Δ = 0.67 ± 0.04), which was used as the reference.[35] No emission signal of singlet oxygen was detected when the solutions where saturated with argon. From the fluorescence excitation spectra, we observed that they closely resemble the absorption spectra, confirming the existence of a single species under the conditions used (1 × 10^{-6} M in DMSO).

The three compounds gave, in DMSO, the typical UV−vis spectra for nonaggregated phthalocyanines showing an intense and sharp Q-band in the red visible region and a Soret band at about 350 nm (Figure 2). The aggregation behavior of these compounds in culture media was also examined by absorption and fluorescence spectroscopic methods. Figure 2 shows the UV−vis spectra of the three PSs in DMEM complete medium for the HeLa cells culture. It can be seen that the Q-band of every compound is much broader than that in DMSO and shifted to the blue region, suggesting that these compounds are aggregated in the medium. However, the Q-band corresponding to GPh3 is slightly different, with a lower value of ε and an additional shoulder at around 690 nm. This fact, together with the fluorescence spectra (data not shown), where no fluorescence emission was observed for GPh1 and GPh2, while GPh3 showed a faint but significant fluorescence in the medium, could be due to a less aggregation behavior of GPh3. From the data shown in Table 1 and in Figure 2, it is reasonable to think that the aggregation tendency of the three compounds in culture media may depend both on the number and the symmetric position of the sugar units.

3.2. *In Vitro* Photodynamic Activities. *3.2.1. Cellular Toxicity.* The toxicity induced by different concentrations of the three PSs (GPh1, GPh2, and GPh3) on HeLa and HaCaT cells, measured with the MTT assay, in the absence of light is shown in Table 2. Treatment of HeLa cells with GPh1 or GPh2 (concentrations of 5 × 10^{-6} M or 1 × 10^{-5} M) or GPh3 (5 × 10^{-7} M or 1 × 10^{-6} M) for 24 h (a much longer time than the incubation time chosen for the rest of experiments) did not induce significant toxicity in HeLa cells, nor in HaCaT cells, indicating that there was not a toxic effect of the PSs at any of the concentrations used on both cell types. To test the effect of red light irradiation alone, we performed control experiments irradiating cells with red light (636 nm) alone with a light dose

dx.doi.org/10.1021/tx300035a | Chem. Res. Toxicol. 2012, 25, 940−951

Table 2. Toxicity Induced in HeLa and HaCaT Cells in the Absence of Light[a]

GPh	concentration (M)	surviving fraction (% ± SD) HeLa	HaCaT
	control	100 ± 4.0	100 ± 3.1
1	5×10^{-6}	110 ± 5.9	96 ± 3.9
	1×10^{-5}	104 ± 14	94 ± 8.2
2	5×10^{-6}	106 ± 6.1	98 ± 9.3
	1×10^{-5}	100 ± 7.7	97 ± 7.7
3	5×10^{-7}	94 ± 6.6	103 ± 3.5
	1×10^{-6}	106 ± 6.1	101 ± 3.9

[a]Cells were incubated for 24 h with different concentrations of GPh1, GPh2, and GPh3. Each value corresponds to the mean obtained from three independent experiments ± standard deviation (SD).

of 11.16 J/cm^2 (the highest light dose used in this work). These conditions did not induce toxicity in both cell lines (96% ± 7.0 or 98% ± 5.0 of cell survival for HeLa or HaCaT cells, respectively).

The toxicity induced by treatment of HeLa cells with 1×10^{-6} M GPh1, GPh2 or even higher concentrations (5×10^{-6} M, not shown) for 4 h followed by variable light doses of red light (636 nm) was very low (Figure 3A). In contrast, treatment of HeLa cells with variable concentrations of GPh3 (1×10^{-6} M in Figure 3A and lower concentrations from 5×10^{-7} M to 1×10^{-8} M in Figure 3B) for 4 h, followed by different times of red light irradiation, resulted in extensive cell toxicity. This effect was dependent on both the concentration and light doses used (1.86−11.16 J/cm^2, Figure 3B). Concentrations of 5×10^{-7} M for 4 h and a light dose of 5.58 J/cm^2 resulted in a nearly 80% decrease of the cell viability. Similar results were obtained for treatments using lower concentration, 1×10^{-7} M for 4 h, but with a light dose of 11.16 J/cm^2 (we assigned these conditions as lethal dose 80, LD80, Figure 3B). Concentrations of 1×10^{-6} M for 4 h and a light dose of 5.58 J/cm^2 resulted in almost 100% of inactive cells (LD100, Figure 3A). Conversely, the phototoxic effects of GPh3 on HaCaT were much lower for the same GPh3 concentrations (for 4 h) and a light dose of 5.58 J/cm^2 (Figure 3C). For example, a high HaCaT surviving percentage of 69.2 ± 7.5% could be reached with 5×10^{-7} M, whereas in HeLa cells, the induced toxicity was of 23.4 ± 5.2%. These results, pointed out that GPh3 provide a good photodynamic effect in HeLa cells with minimal photocytotoxicity to nontumoral cells at the concentrations of GPh3 evaluated.

3.2.2. Subcellular Localization. The subcellular localization of the GPhs in HeLa cells were performed by fluorescence microscopy using the red fluorescence of the compounds under both ultraviolet excitation or green exciting light (Figure 4). For GPh1 and GPh2, no intracellular fluorescence was observed after 4 or 18 h of incubation, with concentrations of 1×10^{-6} and 5×10^{-7} M (data not shown). This fact indicates that the cellular uptake of these compounds is negligible and/or that the compounds could be highly aggregated. In any case, these are good reasons for discontinuing further investigations of the photodynamic effects of GPh1 and GPh2. Furthermore, the MTT assay also corroborates the lack of internalization of these two compounds since they did not show any photocytotoxicity. On the contrary, GPh3 showed very low levels of incorporation inside HeLa cells when incubated with 1×10^{-6} or 5×10^{-7} M for 4 h (almost undetectable, not shown), whereas at 18 h, a significant red fluorescence signal inside cells, corresponding to

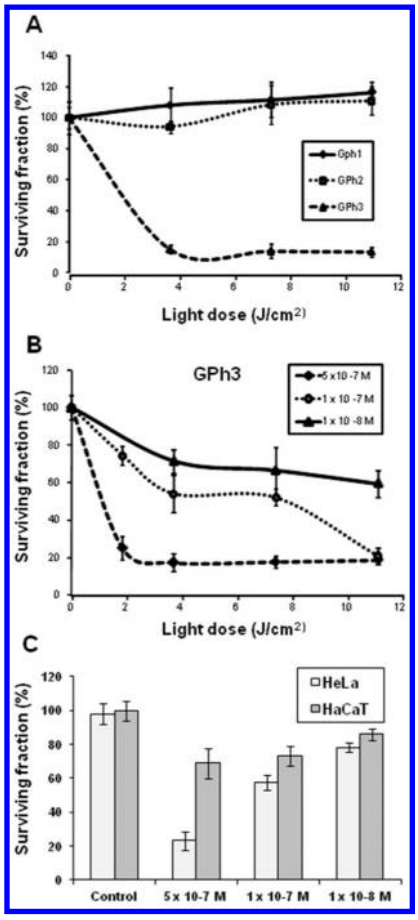

Figure 3. Phototoxicity induced by the glycophthalocyanines in HeLa and HaCaT cells. Toxicity induced by GPh1, GPh2, or GPh3 (1×10^{-6} M) (A) or by GPh3 (5×10^{-7} M, 1×10^{-7} M, or 5×10^{-8} M) (B) on HeLa cells is represented. Cells were incubated with the compounds for 4 h and then were subjected to red light at variable doses. Comparison between the toxicity induced by different concentrations of GPh3 in HeLa or HaCaT cells and subjected to a light dose of 5.58 J/cm^2 (C). MTT assays were performed 48 h after the treatments. Each point corresponds to the mean value ± SD obtained from at least three independent experiments.

GPh3, was detected (Figure 4A,B). Note that in this case, the incubation time of GPh3 is much higher than that in any other experiment. This is because the amount of PS microscopically detected may be greater than that necessary for inducing photodamage. A very low concentration of a given PS within cells may be almost undetectable but able to induce photodynamic effects.[9,11] In any case, after 18 h of incubation, we were able to detect intracellular red fluorescence of GPh3 located at plasma membrane, accumulated near the nucleus and diffused in the cytoplasm. No colocalization with the blue autofluorescence of the mitochondria was observed, and a nuclear localization can be ruled out because nuclei (as seen by phase contrast) do not exhibit red fluorescence due to GPh3 (Figure 4A). These results indicate that GPh3 has a better cellular uptake than GPh1 and GPh2, probably due to its asymmetric structure that provides amphiphilic character leading to lower aggregation tendency within the cells. Co-incubation of the cells with GPh3 and known markers for mitochondria (MTG), lysosomes (LTG), and Golgi apparatus (CellLight Golgi-GFP or NBD-C6) indicated that the fluorescent red area near the nucleus corresponds mainly to

dx.doi.org/10.1021/tx300035a | Chem. Res. Toxicol. 2012, 25, 940−951

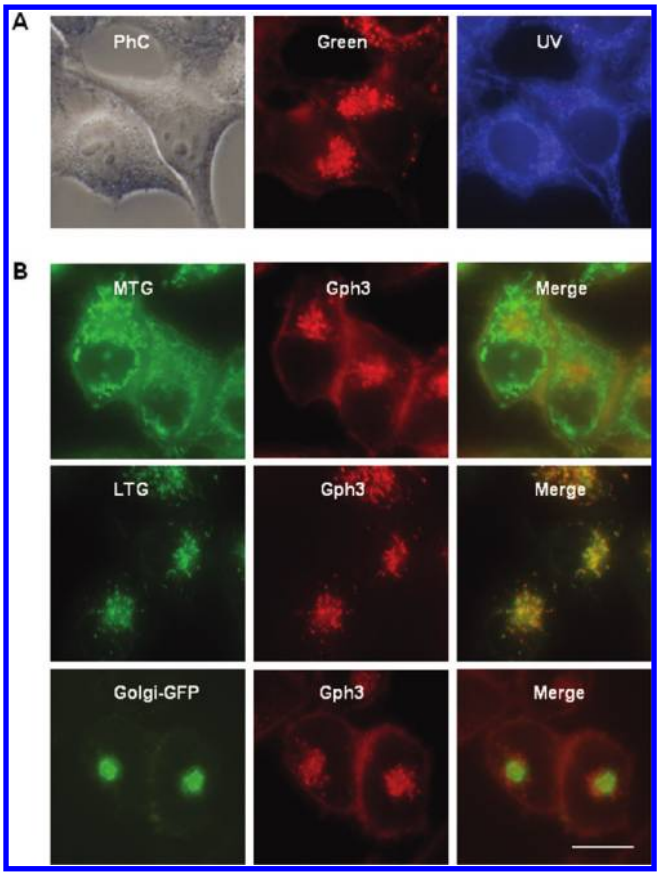

Figure 4. Intracellular localization of GPh3. Cells were incubated with 1×10^{-6} (A) or 5×10^{-7} M (B) of GPh3 for 18 h and then observed with a fluorescence microscope. (A) Cells showed a red fluorescence signal under both UV and green exciting light, mainly at the Golgi apparatus level, although some fluorescence is also observed at the lysosomes, the cell membrane, and diffused into the cytoplasm. (B) Co-incubation of GPh3 with known markers for mitochondria by MitoTracker Green (MTG), lysosomes by Lisotracker Green (LTG), and Golgi apparatus by CellLight Golgi-GFP confirm the localization observed under UV-excitation. Phase contrast (PhC). Scale bar: 20 μm.

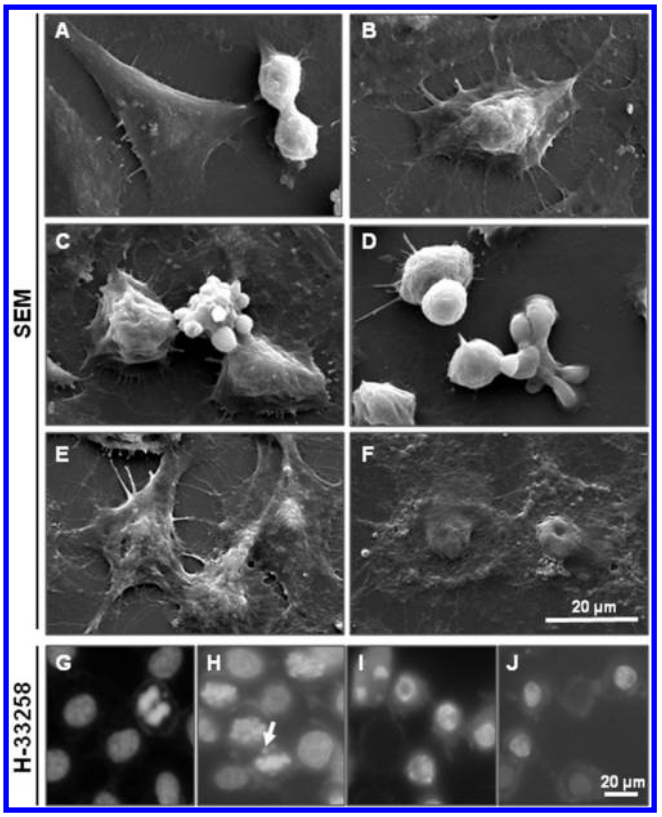

Figure 5. Morphological changes induced by GPh3 and observed by scanning electron microscopy (SEM) or by fluorescence microscopy after staining with H-33258. Control HeLa cells showed a well spread morphology (A) and nuclei with well organized chromatin (G). Three hours after phototreatment (5×10^{-7} M of GPh3 for 4 h and 15 min of red light irradiation), cells appeared retracted (B) and progressively blocked cells in mitosis (H) with chromosomes not aligned in the metaphase plate (arrow). At 24 h (C,I) and 48 h (D) after phototreatment, a significant amount of cells underwent apoptotis. Higher concentrations of GPh3 (1×10^{-6} M) induced necrotic cells clearly distinguished immediately (E) and 24 h (F,J) after phototreatment. Scale bar: 20 μm.

the Golgi apparatus, although some localization could be also in lysosomes (Figure 4B). Since only GPh3 could be seen inside HeLa cells and induced significant photodamage, further studies were performed only with this compound.

3.2.3. Changes in Cell Morphology Induced by PDT with GPh3. HeLa cells observed by scanning electron microscopy or by fluorescence microscopy after staining with H-33258, revealed different morphological changes, depending on the phototreatment conditions selected with GPh3 (Figure 5). Whereas untreated cells showed spread morphology (Figure 5A) and homogeneous nuclei (Figure 5G), photodynamic treatments with LD80 of GPh3 (5×10^{-7} M for 4 h and 15 min of light irradiation, Figure 5B) induced gradual cell retraction, particularly noticeable 3 h after phototreatment. There was also a gradual increase in cells in division indicating that photodynamic treatment with LD80 of GPh3 induced mitotic arrest in HeLa cells (Figure 5H). In addition, a significant increase of apoptotic cells (cell rounding and blebbing, chromatin condensation, typical chromatin fragmentation, and packing into apoptotic bodies[38−40]) could be detected at 24 h (Figure 5C and I) and particularly at 48 h later of photosensitization (Figure 5D). On the contrary, photodynamic treatment with LD100 of GPh3 (1×10^{-6} M for 4 h and 30 min light irradiation) clearly resulted in typical necrotic cell death morphology[38−40] since loss of integrity of the plasma membrane and gradual condensation of chromatin leading pycnotic nuclei were easily recognized both at 3 and 24 h after treatment (Figure 5E, F, and J).

3.2.4. Cell Cytoskeleton Analysis. To further investigate the mechanisms by which GPh3 achieves its effects on HeLa cells, we then studied the changes induced by photodynamic treatment with GPh3 in the cytoskeleton of microtubules (MTs) and actin microfilaments (MFs). These cellular components are directly involved in important cell processes such as division, migration, and invasion.[4] Figure 6 shows immunofluorescence studies for α-tubulin, and it is clearly noted that the mitotic arrest was principally the consequence of a metaphase blockage due to anomalous mitotic spindle arrangement. Control interphase HeLa cells showed a well developed microtubular network and a well organized spindle apparatus in mitosis (Figures 6A and E,E′). Three hours after photodynamic treatment with LD80 of GPh3 (5×10^{-7} M for 4 h and 15 min red light irradiation), the MT network of the cells were altered and disorganized (Figure 6B). Moreover, there was also an increase in the number of dividing cells,

dx.doi.org/10.1021/tx300035a | Chem. Res. Toxicol. 2012, 25, 940−951

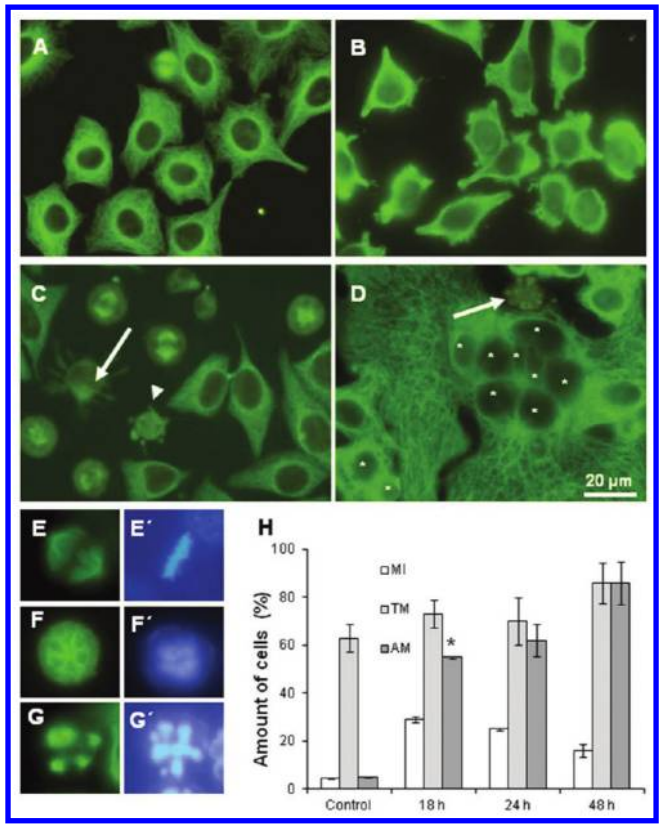

Figure 6. Microtubule damage induced by GPh3. (A) Control HeLa cells showing a well developed network of MTs determined by tubulin immunolabeled and observed by fluorescence microscopy. Three hours after phototreatment (5×10^{-7} M of GPh3 for 4 h and 15 min of red light irradiation) retraction and disorganization of MTs of cells in interphase could be observed (B). At 24 h after phototreatment (C) cells in metaphase showed abnormal mitotic spindles (arrow) as well as cells in apoptosis (arrowhead). At 48 h after phototreatment (D), giant polyploid and multinucleated (asterisks) cells appeared. (E−G) Details of a control (E) and abnormal mitotic spindles of HeLa cells 24 h after phototreatment (F,G). (E′−G′) The chromosomes stained with H-33258 perfectly aligned in the control (E′) or dispersed in the treated metaphase cells (F′,G′). Scale bar: 20 μm. (H) Cell blockage at 18, 24, and 48 h induced after photodynamic treatment with GPh3. MI, mitotic index; TM, total metaphases; AM, abnormal metaphases; data correspond to mean values ± standard deviation from three independent experiments ($*p < 0.05$).

particularly at 18, 24, and 48 h after photodynamic treatment (Figures 6C, F, G, and H). This mitotic arrest was due to an increase in the number of cells stopped in metaphase (metaphase blockage). Most of these cells showed severely altered mitotic spindles (Figure 6C and H), as well as different arrangements of their mitotic poles (Figure 6F,G) and abnormal distribution of chromosomes (Figure 6F′,G′). In many cases, these multipolar metaphases experience an endocycle (a variant cell cycle in which cells undergo repeated rounds of DNA replication with no intervening mitosis), leading to polyploidy and giant cells with multiple nuclei of different sizes (Figure 6D). The amount of these cells increased with time, being 7.6 ± 0.6 and 10.8 ± 0.7, at 24 and 48 h, respectively, after photodynamic treatment, compared to those observed in untreated cultures (0.9 ± 0.3). The most likely origin of these polyploid interphase cells is the abnormal metaphases that have not been properly completed, being remnants of aberrant mitotic processes. Under these experimental conditions, HeLa cell death by apoptosis was evident from 24 h and afterward. Figure 6G and G′ shows the typical morphological features of apoptotic cells after H-33258 staining.

In addition, we have observed that the changes described on MTs induced by photodynamic treatment with GPh3 were accompanied with alterations on another cytoskeleton component: actin MFs (see Supporting Information). GPh3 induced a variable disorganization and reduction in the number of actin filaments compared with the actin pattern of control cells, organized as stress fibers across the cytoplasm (Supporting Information, A). From 1 to 3 h after photodynamic treatment, most of the cells changed the morphology and were retracted (Supporting Information, B); after 24 h, cells showed deformations such as blebs on the cell membrane, and the nuclei showed the characteristic apoptotic chromatin fragmentation (Supporting Information, C,C′). Moreover, multinucleated cells are probably related to failure during cell cycle progression without cytokinesis (Supporting Information, D,D′).

3.2.5. Cell Cycle and Cell Death Analysis. The above results demonstrated that treatment of HeLa cells with GPh3 not only induced severe alterations of the cell cycle but also triggers an apoptotic response. Flow cytometry analysis of the effects induced by photodynamic treatment with GPh3 showed that, in comparison with the DNA content of the control (untreated) cells, cell cycle profiles change for variable incubation times. The experimental conditions used for the flow cytometry analysis were LD80 of GPh3 (1×10^{-7} M or 5×10^{-7} M for 4 h and 30 or 15 min of red irradiation, respectively) and induced similar results under similar conditions. Figure 7 shows the DNA content profile of HeLa cells treated with 5×10^{-7} M of GPh3 for 4 h and 15 min of irradiation. As seen, the cell cycle profiles of treated cells were changed by the accumulation of cells at the G2/M peak, particularly evident 18 and 24 h after treatment (Figure 7B). Flow cytometry measurements (Figure 7B) indicated that 18 and 24 h after photodynamic treatment, about 37% or 28%, respectively, of the cell population, was at G2/M blockage. These results correlated with the microscopic images of the cells, showing that 18 and 24 h after GPh3 treatment, there was an important increase in the number of dividing cells with the disorganized chromatin, confirming mitotic arrest (Figure 5C, D, and H, and Figure 7, 18 and 24 h insets). The mitotic arrest decreased at 48 h (up to 17%), but an increase in the SubG1 fraction (cell death fraction) was clearly detected (43.5%). At this time, an increase in the number of polyploid cells (with a DNA content higher than 4C) was also observed, finding values of 13.4% versus 0.3% in control cells. In addition, a great fraction of the cells was detached from the culture substrate, and after analyzing the nuclear morphology of the supernatant by PI staining, these cells showed apoptotic morphology (Figure 7A, 48 h insert). These results clearly indicate that photodynamic treatment of HeLa cells with LD80 of GPh3 induces severe alterations on the cell cycle, involving mitosis blockage and polyploidy.

We further studied the events related with cell death using the TUNEL assay in both attached and detached cells (Figure 8 A,B). The phase contrast and the fluorescence microscopy images indicated that a significant amount of attached cells were positive to the TUNEL assay both at 24 (around 30%) and 48 h (around 75%). Conversely, the majority of detached cells were positive to the TUNEL reaction at both 24 and 48 h after treatment. These results were quite in accordance with the

dx.doi.org/10.1021/tx300035a | *Chem. Res. Toxicol.* 2012, 25, 940−951

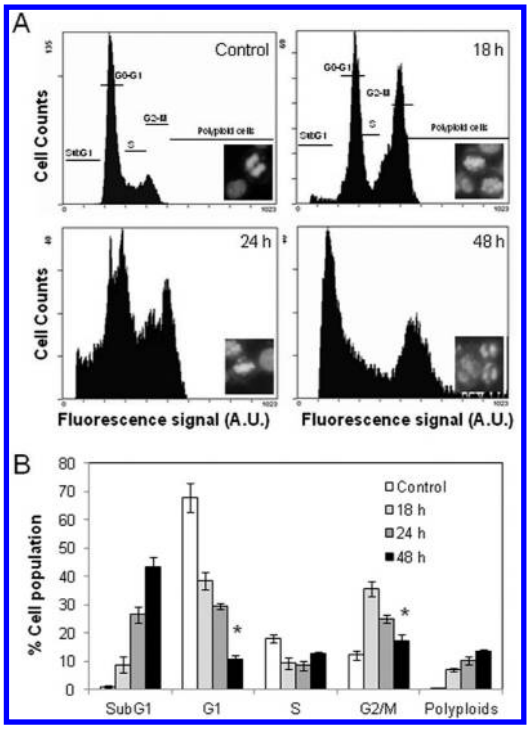

Figure 7. Variations in cell cycle of HeLa cells after phototreatment with GPh3. (A) Flow cytometry analysis 18, 24, and 48 h after phototreatment (5×10^{-7} M of GPh3 for 4 h and 15 min of red light irradiation), compared to control cells. DNA content was measured using propidium iodide (PI). Blockage of cells in G2/M was detected 18 and 24 h after phototreatment, whereas the increase of cell death was clearly visible at 24 and 48 h, concomitantly with the increase of the polyploid population. Insets: HeLa cells visualized by H-33258 for each condition (control, 18, 24, or 48 h after phototreatment). (B) Distribution of cells in the different phases of the cell cycle. Error bars represent the standard deviation of at least three independent experiments (*$p < 0.05$).

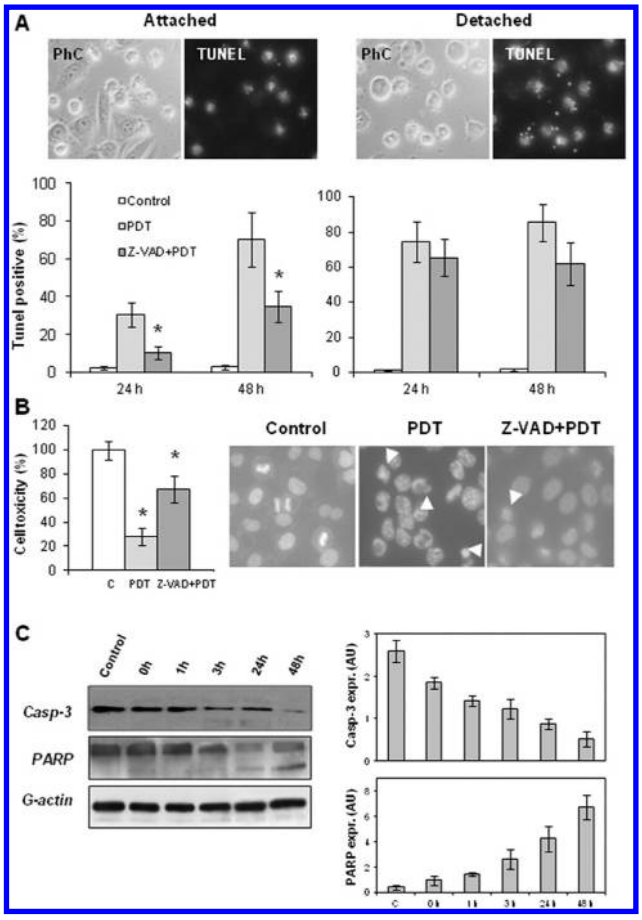

Figure 8. Study of cell death mechanism by the TUNEL assay and Western blot. (A) Cells subjected to LD80 photodynamic treatment and observed under phase contrast (PhC) and under the fluorescence microscope after the TUNEL assay revealed a clear increase of cells in apoptosis with time after the treatment in both attached and detached cells at 24 and 48 h after treatment by estimating the percentage of positive cells to the TUNEL assay. The reactivity to the TUNEL assay was partially abolished by the treatment with Z-VAD prior light irradiation in attached cells (left panel) but did not affect to detached cells (right panel). Error bars represent the standard deviation of three independent experiments (*$p < 0.05$ compared to Z-VAD treated). (B) Cell toxicity induced by the photodynamic treatment with GPh3 (evaluated by the MTT assay) was attenuated by the treatment with Z-VAD prior light irradiation (left panel); error bars represent the standard deviation of three independent experiments (*$p < 0.05$). The morphology of the untreated and treated cells (PDT or Z-VAD-PDT cells) after Hoechst-33258 staining confirms the inhibition of cell death by apoptosis (arrowhead) of Z-VAD. (C) Time-dependent changes in the expression of cell death markers by Western blot when cells were treated with a LD80 of GPh3 and photodynamic treatment (5×10^{-7} M and 15 min of irradiation). Caspase 3 expression decreases in a time-dependent manner and concomitantly with the time-dependent cleavage of 116 kDa PARP in fragments of 89 kDa. G-actin was used as the control for loading. The signal intensity of the caspase 3 and PARP (116 kDa) bands were analyzed by densitometry (arbitrary units, A.U.). Blots shown are from a representative experiment ($n = 3$).

increase of cells in the SubG1 fraction observed by low cytometry. In addition, in a first approach to understand the apoptotic mechanism induced by a LD80 of GPh3, we analyzed the effect of a death broad-spectrum caspase inhibitor, Z-VAD-FMK (Figure 8A,B). Z-VAD-FMK not only reduced the number of TUNEL positive cells in attached cells (around 30% versus 12%) but also increased the general cell viability 48 h after photodynamic treatment (around 22% versus 72% in untreated and treated Z-VAD-FMK, evaluated by the MTT assay).

The implication of caspases in the apoptotic cell death induced by GPh3 was confirmed by Western blot analysis. As can be seen in Figure 8C, the expression of caspase 3 decreases in a time-dependent manner concomitantly with the cleavage of PARP (the main substrate of caspase 3 during apoptosis) from 18 h and afterward (fragments of 89 kDa are formed; Figure 8C). These results indicate that photodynamic treated cells most probably initiate apoptosis after being arrested during mitosis.

Finally, we have also analyzed by Western blot the expression of cyclins B1 and D1 proteins with photodynamic treatment with LD80 of GPh3, compared to control cells (Figure 9). Cyclin B1 is expressed specifically at the G2/M phase during the cell cycle, and it plays a critical role in the progression through mitosis. In this sense, cell cycle progression from G2 to mitosis is accompanied by an accumulation of cyclin B1. However, cyclin D1 is essential for the G1/S transition, also being a marker of cell proliferation. As can be seen in Figure 9, the expression of cyclin B1 decreased immediately and 1 h after photodynamic treatment with GPh3 strongly overexpressed at 3 and 24 h later and decreased again at 48 h after treatment. This peak in the increase of the expression of cyclin B1 at 24 h

dx.doi.org/10.1021/tx300035a | *Chem. Res. Toxicol.* 2012, 25, 940−951

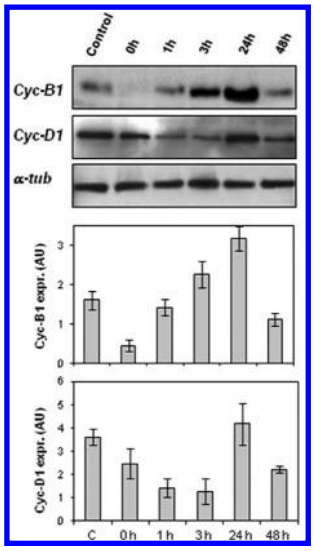

Figure 9. Cyclin determination by Western Blot. Time-dependent changes in the expression of cyclin B1 and D1 by Western blot when cells were treated with a LD80 of GPh3 and photodynamic treatment (5×10^{-7} M and 15 min of irradiation). α-Tubulin was used as the control for loading. The signal intensity of the bands corresponding to cyclin B1 and cyclin D1 was analyzed by densitometry (arbitrary units, A.U.). Blots shown are from a representative experiment ($n = 3$).

may be related with the blockage of cells in division at G2/M phase. With respect to cyclin D1, the same treatment also caused down-regulation of this protein in HeLa cells immediately and during the first hours after the treatment (up to 3 h), and then, its expression was significantly increased at 24 h. These results are completely consistent with the data obtained by flow cytometry, indicating that cells are suffering mitotic arrest.

4. DISCUSSION

The aim of this study is to improve the uptake inside tumor HeLa cells of PSs based on the combination of carbohydrate moieties with phthalocyanine macrocycles and to evaluate their phototoxic effects. Taking into account that cancer cells have increased glucose metabolism to maintain their proliferative rate, the improved cellular incorporation of these PSs will increase the efficiency of PDT. Previous studies have demonstrated that glycosylated silicon(IV) and zinc(II) phthalocyanines show excellent photodynamic activities *in vitro*.[24,36] In this sense, the photophysical properties and photodynamic activities of the three phthalocyanines (GPh1, GPh2, and GPh3) on the human carcinoma cell line HeLa shown in Figure 1 were tested. The results show that, even though all three compounds have relatively high singlet oxygen quantum yield, which is directly involved in cell death induced by PDT,[41−44] only the asymmetric GPh3 was revealed to be photocytotoxic. This fact could be partially explained by the different behavior of the sensitizers in solution, which is a critical parameter for PDT application.[21,43,44] In this sense, the absorption and fluorescence spectroscopic studies showed that aggregation in DMEM is high for the three compounds studied. Nevertheless, the asymmetric GPh3 shows slight, but significant, different absorption and fluorescence characteristics. The asymmetric distribution of the saccharide units on the macrocycle GPh3 possibly prevents the stacking of the individual molecules, being therefore less aggregated than the symmetric GPh1 or GPh2. In addition, the lower photocytotoxicity of GPh1 or GPh2, revealed by the absence of intracellular fluorescence and lower efficiency at generating intracellular ROS, is in agreement with their higher aggregation tendency and/or lower cellular uptake. Moreover, it is likely to presume that the asymmetric chemical structure of GPh3 could behave as an arrowhead pointing to the cell membrane, exhibiting therefore a higher cellular uptake compared to that of GPh1 and GPh2.

The evaluation of the *in vitro* photodynamic effects confirmed that GPh3 showed higher photocytotoxicity effects in HeLa carinoma cells than in nontumoral HaCaT cells. GPh3 is able to induce cell death in HeLa cells by either a necrotic or an apoptotic mechanism, depending on the experimental conditions as other PSs.[39] The cellular changes induced by lethal treatments (LD100, 1×10^{-6} M and a light dose of 11.16 J/cm^2) were severe, and cells died by necrosis immediately after treatment. When using experimental conditions that induced LD80 (1×10^{-7} M or 5×10^{-7} M for 4 h and 11.16 or 5.58 light doses, respectively), cell death occurs mainly by apoptosis, and it does not happen immediately after treatment. Furthermore, photodynamic treatment with LD80 of GPh3 is able to induce metaphase arrest of HeLa cells that ultimately end up in apoptosis. The analysis of the MTs by immunofluorescence evidenced that 18 and 24 h after the phototreatment, mitosis was abnormal, with several multipolar metaphases and chromosomes scattered around the mitotic spindle. At this time, G2/M arrest was also observed by flow cytometry. Forty-eight hours after phototreatment, a great fraction of the cells were in apoptosis, as detected by flow cytometry and TUNEL assay. Apoptotic cell death was also confirmed by studying nuclear morphology with H-33258 staining, which evidenced the characteristic condensation and fragmentation of the chromatin observed by fluorescence.

Since photodynamic treatment with GPh3 is able to induce the formation of aberrant mitosis and multinucleated cells, mitotic catastrophe could probably be the main mechanism by which this compound triggers apoptosis in HeLa cells. The same cellular alterations described here have also been reported by other authors regarding mitotic catastrophe followed by apoptosis after photodynamic therapy.[45−48] Although its molecular mechanism is not completely known, mitotic catastrophe can explain cell death induced by treatments that cause aberrant mitosis, when the G2 checkpoint is defective and cells enter in mitosis before DNA damage has been repaired.[40,49] Cells proceed with mitosis and cycle into G1 without achieving cytokinesis and becoming multinucleated and polyploid. In some cases, cells undergo cytokinesis with an incomplete separation of the chromosomes. This is particularly known to occur after treatment with different products that disturb the dynamics of MTs either by depolymerization (e.g., nocodazol) or by stabilization (e.g., taxol) or topoisomerase II inhibitors.[49] Abnormal disjunction of chromosomes around the mitotic spindle on HeLa cells and configuration of multinucleated and poliploid cells has been already described.[6,11,49,50]

In addition to the GPh3-induced modifications on MTs, alterations in actin MFs have been also observed. MFs are a crucial target for anticancer compounds such as cytochalasins. These severe changes in actin MFs are probably the cause of cytokinesis inhibition, generating therefore multinuclear globular giant cells. Similar results to those described here for MTs and MFs by GPh3 have been described after PDT of

HeLa cells with ZnPc[4,11] or for other cell types in response to photosensitization with other PSs.[9] In any case, the relevance of these cytoskeletal components involved in cell photokilling is obvious, and thus, they are important targets for PDT of cancer.

In agreement with microscopic observations, the TUNEL assay showed an increased amount of apoptotic cells with time after photodynamic treatment. This effect was partially inhibited by the treatment with the broad-caspase inhibitor Z-VAD-FMK prior to irradiation. Western blot analysis, however, clearly indicated a decrease of caspase 3 expression and cleavage of PARP from 24 h after phototreatment, concomitantly with the increased amount of apoptotic cells detected by TUNEL and with the changes in the cell cycle observed by flow cytometry. Taken together, the data presented indicate that cell death induced by photodynamic treatment with the LD80 of GPh3 is mainly by apoptosis but that it is not entirely caspase-dependent, and other cell death pathways could be implicated. Further studies to better understand the implication of caspases in the cell death apoptotic mechanism induced by photodynamic treatment with GPh3 are underway.

We have also analyzed the protein expression of cyclin B1 and cyclin D1 measured by Western blot, which was increased 24 h after phototreatment followed by a decrease in expression at 48 h. Throughout the cell cycle, cyclin B1 operates either at the spindle assembly checkpoint or during later mitotic events, being particularly critical for the maintenance of the mitotic state.[51] In this sense, an increase in the expression of cyclin B1 has been described to be clearly induced in HeLa cells treated with different compounds, such as the MT depolymerizing drug noncodazole and topoisomerase II inhibitors, known to induce mitotic arrest in this cell line.[52,53] Biphasic response of cyclin B1 has been described after PDT with other photosensitizers such as hypericin also in HeLa cells.[45] Cyclin D1 is a protein which is one of the most frequently altered cell cycle regulators in human tumors, often being overexpressed in transformed cells.[54,55] Although GPh3 induced a partial downregulation of cyclin D1 during the first hours, the expression of this protein markedly increased 24 h after phototreatment. As far as we know, these results demonstrate for the first time the biphasic response of cyclin D1 after PDT since, conversely, other authors have reported a downregulation of cyclin D1 expression with time after photodynamic therapy.[56,57] The discrepancy with our results could be due to, among other factors, the cell type (bladder or colon carcinoma cells vs cervical carcinoma cells), the photosensitizer (Hypericin vs GPh3), or even the experimental conditions used.

We would also like to point out that photosensitization reactions are highly dependent on the subcellular location of the PSs.[41,42] Singlet oxygen-induced photodamage is highly localized, and although its lifetime is long enough to diffuse over long distances within the cells, the initial oxidative reactions first occur in organelles in which PSs are located (and to some extent in other cell structures) leading altogether to cell photoinactivation. Thus, the damage we have observed in cytoskeletal elements (responsible for the blockage of mitosis and the inhibition of cytokinesis) could be induced either directly by the binding of GPh3 to the cytoskeletal proteins or indirectly by the generation of ROS.[6,7] Since the intracellular localization of GPh3 seems to be mainly on membranes (plasma membrane, lysosomes, and Golgi apparatus), additional experiments must be done to understand the influence of the localization and the induction of cell death by apoptosis through mitotic catastrophe.

In conclusion, we have established that the presence of carbohydrate moieties provides solubility to the PSs in physiological fluids and improves cellular uptake. Furthermore, our results demonstrate that the asymmetric substitution of the sugars on the macrocycle GPh3 is crucial to prevent the aggregation tendency of the individual molecules, when compared with symmetric GPh1 or GPh2. Although GPh3 is somewhat aggregated in the culture medium, it has a better cellular uptake, probably due to its amphiphilic character. Additional studies on GPh1 and GPh2 are needed to reduce their aggregation *in vitro* either using a carrier system or by the addition of detergents (such as polysorbates, Cremophor EL, polyethylene glycol, or lipid emulsions). With respect to the mechanisms of action of the PDT with GPh3, we have demonstrated that the LD80 causes a sequence of harmful events in HeLa cells, starting with alteration of MTs (with anomalous chromosome pairing during mitosis), followed by multipolar spindles, metaphase blockage, and finally mitotic catastrophe, with the resulting apoptotic cell death. Actin MFs are also affected by photodynamic treatment with GPh3, although their contribution to the cell death process needs to be further evaluated. Our results clearly indicate that GPh3, probably because of its asymmetric and amphiphilic structure, could be potentially used as an efficient generator of intracellular ROS, as well as an interesting PS for further studies regarding PDT.

■ ASSOCIATED CONTENT

Supporting Information

GPh3-induced photomodifications on actin microfilaments. This material is available free of charge via the Internet at http://pubs.acs.org.

■ AUTHOR INFORMATION

Corresponding Author

*Departamento de Biologia, Facultad de Ciencias, Universidad Autónoma de Madrid, Canto Blanco, E-28049 Madrid, Spain. Phone: +34 91 497 8247. Fax: +34 91 497 8344. E-mail: angeles.juarranz@uam.es.

Funding

The work was supported by a grant from MICINN and MEC (FIS, PS09/01099; CTQ-2011-24187/BQU), Comunidad de Madrid (S2010/BMD-2359; MADRISOLAR-2; S2009/PPQ/1533), and Consolider-Ingenio Nanociencia Molecular (CSD2007-00010), Spain. A.R.M.S. is grateful to FCT (Fundação para a Ciência e a Tecnologia, Portugal) for her doctoral grant (SFRH/BD/29362/2006). D.M.G. gratefully acknowledges financial support by the DFG (SFB 583) and FCI.

Notes

The authors declare no competing financial interest.

■ ACKNOWLEDGMENTS

We recognize the valuable contribution by Carmen Moreno Ortiz (Flow Cytometry Service, Centro Nacional de Biotecnología, Madrid) and Esperanza Salvador (Scanning Electron Microscopy Laboratory, Universidad Autónoma de Madrid).

■ ABBREVIATIONS

PDT, photodynamic therapy; PS, photosensitizer; ROS, reactive oxygen species; PCI, photochemical internalization; $^1O_2$, singlet oxygen; MT, microtubules; MF, microfilaments; ZnPc, zinc(II) phthalocyanines; DMEM, Dulbecco's modified Eagle's medium; Z-VAD-FMK, benzylocarbonyl-Val-Ala-Asp-fluoromethyl ketone

■ REFERENCES

(1) Agostinis, P., Berg, K., Cengel, K. A., Foster, T. H., Girotti, A. W., Gollnick, S. O., Hahn, S. M., Hamblin, M. R., Juzeniene, A., Kessel, D., Korbelik, M., Moan, J., Mroz, P., Nowis, D., Piette, J., Wilson, B. C., and Golab, J. (2011) Photodynamic therapy of cancer: an update. *CA Cancer. J. Clin. 61*, 250−81.

(2) Dolmans, D. E., Fukumura, D., and Jain, R. K. (2003) Photodynamic therapy for cancer. *Nat. Rev. Cancer 3*, 380−387.

(3) Juarranz, A., Jaen, P., Sanz-Rodriguez, F., Cuevas, J., and Gonzalez, S. (2008) Photodynamic therapy of cancer. Basic principles and applications. *Clin. Transl. Oncol. 10*, 148−154.

(4) Dumontet, C., and Jordan, M. A. (2010) Microtubule-binding agents: a dynamic field of cancer therapeutics. *Nat. Rev. Drug Discovery 9*, 790−803.

(5) Juarranz, A., Espada, J., Stockert, J. C., Villanueva, A., Polo, S., Dominguez, V., and Canete, M. (2001) Photodamage induced by Zinc(II)-phthalocyanine to microtubules, actin, alpha-actinin and keratin of HeLa cells. *Photochem. Photobiol. 73*, 283−289.

(6) Galaz, S., Espada, J., Stockert, J. C., Pacheco, M., Sanz-Rodriguez, F., Arranz, R., Rello, S., Canete, M., Villanueva, A., Esteller, M., and Juarranz, A. (2005) Loss of E-cadherin mediated cell-cell adhesion as an early trigger of apoptosis induced by photodynamic treatment. *J. Cell. Physiol. 205*, 86−96.

(7) Uzdensky, A., Kolpakova, E., Juzeniene, A., Juzenas, P., and Moan, J. (2005) The effect of sub-lethal ALA-PDT on the cytoskeleton and adhesion of cultured human cancer cells. *Biochim. Biophys. Acta 1722*, 43−50.

(8) Stockert, J. C., Canete, M., Juarranz, A., Villanueva, A., Horobin, R. W., Borrell, J. I., Teixido, J., and Nonell, S. (2007) Porphycenes: facts and prospects in photodynamic therapy of cancer. *Curr. Med. Chem. 14*, 997−1026.

(9) Espada, J., Galaz, S., Sanz-Rodriguez, F., Blazquez-Castro, A., Stockert, J. C., Bagazgoitia, L., Jaen, P., Gonzalez, S., Cano, A., and Juarranz, A. (2009) Oncogenic H-Ras and PI3K signaling can inhibit E-cadherin-dependent apoptosis and promote cell survival after photodynamic therapy in mouse keratinocytes. *J. Cell. Physiol. 219*, 84−93.

(10) Piette, J., Volanti, C., Vantieghem, A., Matroule, J. Y., Habraken, Y., and Agostinis, P. (2003) Cell death and growth arrest in response to photodynamic therapy with membrane-bound photosensitizers. *Biochem. Pharmacol. 66*, 1651−9.

(11) Rello-Varona, S., Stockert, J. C., Canete, M., Acedo, P., and Villanueva, A. (2008) Mitotic catastrophe induced in HeLa cells by photodynamic treatment with Zn(II)-phthalocyanine. *Int. J. Oncol. 32*, 1189−1196.

(12) Wainwright, M. (2008) Photodynamic therapy: the development of new photosensitisers. *Anticancer Agents Med. Chem. 8*, 280−291.

(13) Allen, C. M., Sharman, W. M., and Van Lier, J. E. (2001) Current status of phthalocyanines in the photodynamic therapy of cancer. *J. Porphyrins Phthalocyanines 5*, 161−169.

(14) Lo, P. C., Fong, W. P., and Ng, D. K. (2008) Effects of peripheral chloro substitution on the photophysical properties and in vitro photodynamic activities of galactose-conjugated silicon(IV) phthalocyanines. *ChemMedChem 3*, 1110−1117.

(15) Durmus, M., and Ahsen, V. (2010) Water-soluble cationic gallium(III) and indium(III) phthalocyanines for photodynamic therapy. *J. Inorg. Biochem. 104*, 297−309.

(16) Zhou, C., Shunji, C., Jinsheng, D., Junlin, L., Jori, G., and Milanesi, C. (1996) Apoptosis of mouse MS-2 fibrosarcoma cells induced by photodynamic therapy with Zn (II)-phthalocyanine. *J. Photochem. Photobiol., B 33*, 219−223.

(17) Cristobal, J., Stockert, J. C., Villanueva, A., Rello-Varona, S., Juarranz, A., and Canete, M. (2006) Caspase-2: a possible trigger of apoptosis induced in A-549 tumor cells by ZnPc photodynamic treatment. *Int. J. Oncol. 28*, 1057−1063.

(18) Allen, C. M., Langlois, R., Sharman, W. M., La Madeleine, C., and Van Lier, J. E. (2002) Photodynamic properties of amphiphilic derivatives of aluminum tetrasulfophthalocyanine. *Photochem. Photobiol. 76*, 208−216.

(19) Sharma, S. K., Dai, T., Kharkwal, G. B., Huang, Y. Y., Huang, L., De Arce, V. J., Tegos, G. P., and Hamblin, M. R. (2011) Drug discovery of antimicrobial photosensitizers using animal models. *Curr. Pharm. Des. 17*, 1303−1319.

(20) Garland, M. J., Cassidy, C. M., Woolfson, D., and Donnelly, R. F. (2009) Designing photosensitizers for photodynamic therapy: strategies, challenges and promising developments. *Future Med. Chem. 1*, 667−691.

(21) Qiu, T., Xu, X., Liu, J., and Qian, X. (2009) Novel perfluoroalkyl phthalocyanine metal derivatives: Synthesis and photodynamic activities. *Dyes Pigm. 83*, 127−133.

(22) Sharman, W. M., and Van Lier, J. E. (2005) A new procedure for the synthesis of water-soluble tri-cationic and -anionic phthalocyanines. *J. Porphyrins Phthalocyanines 9*, 651−659.

(23) Ribeiro, A. O., Tomé, J. P. C, Neves, M. G. P. M. S., Tomé, A. C., Cavaleiro, J. A. S., and Iamamoto, Y. (2006) [1,2,3,4-tetrakis-(alpha/beta-D-galactopyranos-6-yl)-phthalocyaninato]zinc(II): a water-soluble phthalocyanine. *Tetrahedron Lett. 47*, 9177−9180.

(24) Choi, C. F., Huang, J. D., Lo, P. C., Fong, W. P., and Ng, D. K. (2008) Glycosylated zinc(II) phthalocyanines as efficient photosensitisers for photodynamic therapy. Synthesis, photophysical properties and in vitro photodynamic activity. *Org. Biomol. Chem. 6*, 2173−2181.

(25) Soares, A. R., Tome, J. P., Neves, M. G. P. M. S., Tome, A. C., Cavaleiro, J. A., and Torres, T. (2009) Synthesis of water-soluble phthalocyanines bearing four or eight D-galactose units. *Carbohydr. Res. 344*, 507−510.

(26) Liu, J. Y., Lo, P. C., Fong, W. P., and Ng, D. K. (2009) Effects of the number and position of the substituents on the in vitro photodynamic activities of glucosylated zinc(II) phthalocyanines. *Org. Biomol. Chem. 7*, 1583−1591.

(27) Berg, K., Weyergang, A., Prasmickaite, L., Bonsted, A., Hogset, A., Strand, M. T., Wagner, E., and Selbo, P. K. (2010) Photochemical internalization (PCI): a technology for drug delivery. *Methods Mol. Biol. 635*, 133−145.

(28) Selbo, P. K., Weyergang, A., Hogset, A., Norum, O. J., Berstad, M. B., Vikdal, M., and Berg, K. (2010) Photochemical internalization provides time- and space-controlled endolysosomal escape of therapeutic molecules. *J. Controlled Release 148*, 2−12.

(29) Josefsen, L. B., and Boyle, R. W. (2008) Photodynamic therapy: novel third-generation photosensitizers one step closer? *Br. J. Pharmacol. 154*, 1−3.

(30) Tuncel, S., Dumoulin, F., Gailer, J., Sooriyaarachchi, M., Atilla, D., Durmus, M., Bouchu, D., Savoie, H., Boyle, R. W., and Ahsen, V. (2010) A set of highly water-soluble tetraethyleneglycol-substituted Zn(ii) phthalocyanines: synthesis, photochemical and photophysical properties, interaction with plasma proteins and in vitro phototoxicity. *Dalton Trans. 40*, 4067−4079.

(31) Dwek, R. A. (1996) Glycobiology: Toward understanding the function of sugars. *Chem. Rev. 96*, 683−720.

(32) Liu, J. Y., Lo, P. C., Jiang, X. J., Fong, W. P., and Ng, D. K. (2009) Synthesis and in vitro photodynamic activities of di-alpha-substituted zinc(ii) phthalocyanine derivatives. *Dalton Trans. 21*, 4129−4135.

(33) Zheng, G., Graham, A., Shibata, M., Missert, J. R., Oseroff, A. R., Dougherty, T. J., and Pandey, R. K. (2001) Synthesis of α-galactose-conjugated chlorins derived by enyne metathesis as galectin-specific photosensitizers for photodynamic therapy. *J. Org. Chem. 66*, 8709−8716.

(34) Vedachalam, S., Choi, B., Pasunooti, K. K., Ching, K. M., Lee, K., Yoon, H. S., and Liu, X. W. (2011) Glycosylated porphyrin derivatives and their photodynamic activity in cancer cells. *Med. Chem. Commun. 2*, 371−377.
(35) Williams, A. T. R., Winfield, S. A., and Miller, J. N. (1983) Relative fluorescence quantum yields using a computer-controlled luminescence spectrometer. *Analyst 108*, 1067−1071.
(36) Villanueva, A., Dominguez, V., Polo, S., Vendrell, V. D., Sanz, C., Canete, T. M., Juarranz, A., and Stockert, J. C. (1999) Photokilling mechanisms induced by zinc(II)-phthalocyanine on cultured tumor cells. *Oncol. Res. 11*, 447−453.
(37) Mosmann, T. (1983) Rapid colorimetric assay for cellular growth and survival: application to proliferation and cytotoxicity assays. *J. Immunol. Methods 65*, 55−63.
(38) Seotsanyana-Mokhosi, I., Kuznetsova, N., and Nyokong, T. (2001) Photochemical studies of tetra-2,3-pyridinoporphyrazines. *J. Photochem. Photobiol., A 140*, 215−222.
(39) Rello, S., Stockert, J. C., Moreno, V., Gamez, A., Pacheco, M., Juarranz, A., Canete, M., and Villanueva, A. (2005) Morphological criteria to distinguish cell death induced by apoptotic and necrotic treatments. *Apoptosis 10*, 201−208.
(40) Kroemer, G., Galluzzi, L., Vandenabeele, P., Abrams, J., Alnemri, E. S., Baehrecke, E. H., Blagosklonny, M. V., El-Deiry, W. S., Golstein, P., Green, D. R., Hengartner, M., Knight, R. A., Kumar, S., Lipton, S. A., Malorni, W., Nunez, G., Peter, M. E., Tschopp, J., Yuan, J., Piacentini, M., Zhivotovsky, B., and Melino, G. (2009) Classification of cell death: recommendations of the Nomenclature Committee on Cell Death 2009. *Cell Death Differ. 16*, 3−11.
(41) Jiménez-Banzo, A., Sagristá, M. L., Mora, M., and Nonell, S. (2008) Kinetics of singlet oxygen photosensitization in human skin fibroblasts. *Free Radical Biol. Med. 44*, 1926−1934.
(42) Da Silva, E. F. F., Pedersen, B. W., Breitenbach, T., Toftegaard, R., Kuimova, M. K., Arnaut, L. G., and Ogilby, P. R. (2012) Irradiation- and sensitizer-dependent changes in the lifetime of intracellular singlet oxygen produced in a photosensitized process. *J. Phys. Chem. B 116*, 445−461.
(43) Dhami, S., and Phillips, D. (1996) Comparison of the photophysics of an aggregating and non-aggregating aluminium phthalocyanine system incorporated into unilamellar vesicles. *J. Photochem. Photobiol., A 100*, 77−84.
(44) Koval'skaya, N. E., Kuznetsova, N. A., Kaliya, O. L., Gretsova, N. S., and Sokolova, I. V. (2001) The efficiency of the formation of singlet oxygen by a sensitizer based on zinc phthalocyanine. *J. Appl. Spectrosc. 68*, 287−290.
(45) Vantieghem, A., Xu, Y., Assefa, Z., Piette, J., Vandenheede, J. R., Merlevede, W., De Witte, P. A., and Agostinis, P. (2002) Phosphorylation of Bcl-2 in G2/M phase-arrested cells following photodynamic therapy with hypericin involves a CDK1-mediated signal and delays the onset of apoptosis. *J. Biol. Chem. 277*, 37718−37731.
(46) Piette, J., Volanti, C., Vantieghem, A., Matroule, J. Y., Habraken, Y., and Agostinis, P. (2003) Cell death and growth arrest in response to photodynamic therapy with membrane-bound photosensitizers. *Biochem. Pharmacol. 66*, 1651−1659.
(47) Ferenc, P., Solár, P., Kleban, J., Mikes, J., and Fedorocko, P. (2010) Down-regulation of Bcl-2 and Akt induced by combination of photoactivated hypericin and genistein in human breast cancer cells. *J. Photochem. Photobiol., 98*, 25−34.
(48) Compagnin, C., Mognato, M., Celotti, L., Canti, G., Palumbo, G., and Reddi, E. (2010) Cell proliferation and cell cycle alterations in oesophageal p53-mutated cancer cells treated with cisplatin in combination with photodynamic therapy. *Cell Proliferation 43*, 262−74.
(49) Portugal, J., Mansilla, S., and Bataller, M. (2000) Mechanisms of drug-induced mitotic catastrophe in cancer cells. *Curr. Pharm. Des. 16*, 69−78.
(50) Wu, Y. C., Yen, W. Y., Ho, H. Y., Su, T. L., and Yih, L. H. (2010) Glyfoline induces mitotic catastrophe and apoptosis in cancer cells. *Int. J. Cancer 126*, 1017−1028.
(51) Mena, A. L., Lam, E. W., and Chatterjee, S. (2010) Sustained spindle-assembly checkpoint response requires de novo transcription and translation of cyclin B1. *PLoS One 5* (9), e13037.
(52) Gong, D., and Ferrell, J. E. Jr. (2010) The roles of cyclin A2, B1, and B2 in early and late mitotic events. *Mol. Biol. Cell 21*, 3149−3161.
(53) Sabisz, M., Wesierska-Gadek, J., and Skladanowski, A. (2010) Increased cytotoxicity of an unusual DNA topoisomerase II inhibitor compound C-1305 toward HeLa cells with downregulated PARP-1 activity results from re-activation of the p53 pathway and modulation of mitotic checkpoints. *Biochem. Pharmacol. 79*, 1387−1397.
(54) Kim, J. K., and Diehl, J. A. (2009) Nuclear cyclin D1: an oncogenic driver in human cancer. *J. Cell. Physiol. 220*, 292−296.
(55) Witzel, I. I., Koh, L. F., and Perkins, N. D. (2010) Regulation of cyclin D1 gene expression. *Biochem. Soc. Trans. 38*, 217−222.
(56) Bhuvaneswari, R., Gan, Y. Y., Soo, K. C., and Olivo, M. (2009) Targeting EGFR with photodynamic therapy in combination with Erbitux enhances in vivo bladder tumor response. *Mol. Cancer 8*, 94.
(57) Ozmen, A., Bauer, S., Gridling, M., Singhuber, J., Krasteva, S., Madlener, S., Vo, T. P., Stark, N., Saiko, P., Fritzer-Szekeres, M., Szekeres, T., Askin-Celik, T., Krenn, L., and Krupitza, G. (2009) In vitro anti-neoplastic activity of the ethno-pharmaceutical plant *Hypericum adenotrichum* Spach endemic to Western Turkey. *Oncol. Rep. 22*, 845−852.